Clinical Radiology 74 (2019) 895.e17–895.e26

Contents lists available at ScienceDirect

Clinical Radiology

journal homepage: www.clinicalradiologyonline.net

Diagnostic performance of multiparametric MRI parameters for Gleason score and cellularity metrics of prostate cancer in different zones: a quantitative comparison

J. Gao [a,1], Q. Zhang [a,1], C. Zhang [a,1], M. Chen [a], D. Li [b], Y. Fu [c], X. Lv [a], B. Zhang [b,*], H. Guo [a,*]

[a] *Department of Urology, Nanjing Drum Tower Hospital, The Affiliated Hospital of Nanjing University Medical School, Institute of Urology Nanjing University, 321 Zhongshan Rd, Nanjing, Jiangsu, China*
[b] *Department of Radiology, Nanjing Drum Tower Hospital, The Affiliated Hospital of Nanjing University Medical School, Nanjing, Jiangsu, China*
[c] *Department of Pathology, Nanjing Drum Tower Hospital, The Affiliated Hospital of Nanjing University Medical School, Nanjing, Jiangsu, China*

ARTICLE INFORMATION

Article history:
Received 12 April 2019
Accepted 21 June 2019

AIM: To compare the diagnostic performance of multiparametric MRI (mpMRI) parameters for Gleason score (GS) and cellularity metrics of prostate cancer (PCa) in the peripheral zone (PZ) and transition zone (TZ) separately.

MATERIALS AND METHODS: In total, 225 PCa patients with preoperative mpMRI and whole-mount pathological sections were enrolled retrospectively. Detection rates of index lesions (highest GS or largest dimension) and clinically significant PCa (csPCa) were evaluated. Tumour-to-muscle ratio and skewness of T2 signal intensity, average apparent diffusion coefficient (ADC_{mean}) and 10th percentile ADC ($ADC_{10\%}$) were derived and correlation with GS was performed with Spearman's correlation coefficient (ρ), while effectiveness in differentiating GS 6 from GS ≥7 was compared with receiver operating characteristic (ROC) analysis. Moreover, correlation of cellularity metrics with mpMRI parameters was evaluated with Pearson's correlation coefficient (r).

RESULTS: In total, 398 lesions were identified, with 87.1% (196/225) index lesions and 86.8% (249/287) csPCa detected. Compared to T2 parameters, ADC parameters, especially ADC_{mean}, correlated better with GS (maximal ρ: −0.58 versus −0.33, p=0.011) and yielded significantly higher area under the curve (AUC) in differentiating GS 6 from GS ≥7 (maximal AUC: 0.854 versus 0.731, p=0.020) among PZ lesions. Moreover, ADC_{mean} demonstrated significantly moderate correlation with the nuclear-to-cytoplasmic ratio and nuclear fraction (r=−0.403 and −0.514, p<0.001); however, for TZ lesions, all parameters demonstrated poor correlation with GS and cellularity metrics.

* Guarantor and correspondent: H. Guo and B. Zhang, No. 321 Zhongshan Road, Nanjing, 210008, Jiangsu Province, China. Tel.: +862583106666; fax: +862568182863.
E-mail addresses: zhangbing_nanjing@vip.163.com (H. Zhang), dr.ghq@nju.edu.cn (H. Guo).
[1] These authors contributed equally to this work.

https://doi.org/10.1016/j.crad.2019.06.012

CONCLUSION: mpMRI could effectively detect index and csPCa lesions. ADC parameters, especially ADC_{mean}, correlated better with GS and cellularity metrics than T2 in PZ, while all parameters demonstrated poor performance within TZ lesions.

Introduction

Prostate cancer (PCa), the most common cancer type and a major cause of cancer mortality for men in Europe and the United States, is a histologically heterogeneous and frequently multifocal disease.[1,2] Clinically significant PCa (csPCa) is a lesion that has potential to progress if with no treatment is given and the index tumour (the lesion with the highest Gleason score [GS]) might be the source of progenitor cells responsible for generating metastatic disease.[3–5] Multiparametric magnetic resonance imaging (mpMRI) is currently the best imaging method to non-invasively identify and characterise PCa.[6] Level 1 evidence recently proved mpMRI to improve csPCa diagnosis, decrease unnecessary biopsies, and reduce non-significant PCa diagnosis.[7,8] Moreover, parameters derived from pre-operative mpMRI could effectively differentiate high-risk PCa (local advanced or PSA >20 ng/ml or GS >7 or cT2c) from low-risk PCa (PSA <10 ng/ml and GS <7 and cT1–2a).[9,10]

Several studies have previously analysed some effective parameters of T2-weighted imaging (T2WI) or diffusion-weighted imaging (DWI) for differentiation of PCa from normal prostatic tissue or evaluation of tumour aggressiveness, such as tumour-to-muscle T2 signal intensity (SI) ratio ($T2_{ratio}$),[11] T2 SI skewness ($T2_{skewness}$),[12,13] average apparent diffusion coefficient (ADC_{mean}),[13,14] 10th percentile ADC ($ADC_{10\%}$)[12,14] and whole-prostate ADC ratio.[15] As for PCa aggressiveness evaluation, lower $T2_{ratio}$ was associated with higher Gleason grade.[11] Simultaneously, ADC_{mean} and $ADC_{10\%}$ have shown significantly inverse correlation with pathological GS[13,14,16]; however, limited studies have compared these parameters and the results were not concordant.[11,12] In addition, different diagnostic patterns were recommended between lesions of the peripheral zone (PZ) and transition zone (TZ) according to the guideline,[6] while most of the previous studies took them as a whole. Hence, a larger sample size is needed for comparison among these parameters on sub-region analysis. In addition, using whole-mount sections as the reference standard allows an exact match between MRI and radical prostatectomy (RP) specimens, while most of the previous studies used biopsy pathology or routine RP specimens as the reference standard.

Apart from GS, cellularity metrics can also reflect the proliferative activity and aggressiveness of PCa.[17] Generally, PCa is histologically characterised with enlarged nucleus, amphophilic cytoplasm, and increased cellular density in the epithelial lining of the lumen.[18] Some cellularity metrics including nuclear fraction were significantly increased in PCa compared with normal prostate tissue.[19,20] Simultaneously, the nuclei of Gleason grade 4 from GS 4+3 were significantly larger than those from GS 3+4.[21] Several studies revealed significant correlation between measured ADC value and nuclear fraction,[20,22] but rarely have studies focused on the nuclear-to-cytoplasmic ratio (NCR).

The aim of the present study was to compare the relation of mpMRI parameters with PCa aggressiveness (index tumour, csPCa, GS, and cellularity metrics) on sub-region analysis with a relatively larger patient group using whole-mount sections, which might be useful for targeted biopsy, focal therapy, and active surveillance.

Materials and methods

Patients

Medical data of patients with PCa were reviewed retrospectively with inclusion criteria as follows: (a) prostate mpMRI examination was performed at 3 T; (b) patients underwent RP within 6 months of MRI and had a histopathological diagnosis of prostate adenocarcinoma; (c) complete whole-mount prostate sections were available; (d) no neoadjuvant therapy (hormone or radiotherapy) was given before surgery. Between January 2017 and June 2018, 257 consecutive patients were preliminarily selected for further screening, and the excluded patients are summarised in Fig 1. Finally, after exclusions 225 patients were enrolled. The institutional ethics committee approval was

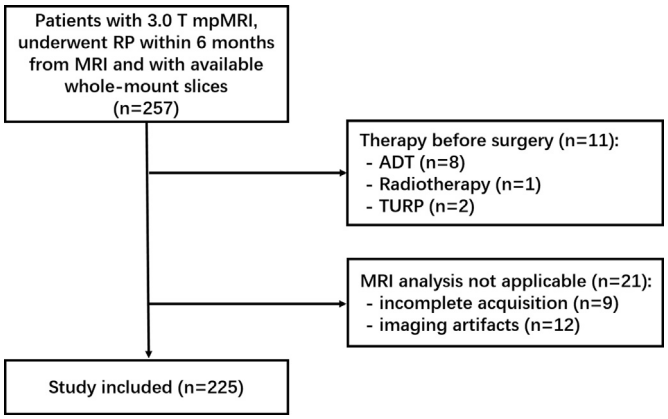

Figure 1 Flowchart of patient selection. mpMRI, multiparametric MRI; RP, radical prostatectomy; ADT, androgen deprivation therapy; TURP, transurethral resection of prostate.

obtained and all patients were informed and signed consent.

MRI acquisition

Multiparametric prostate MRI examinations were performed using a 3 T MRI system (Achieva 3.0 T, Philips Medical Systems, The Netherlands) by using a 32-channel phased-array coil. No endorectal coil was used. Turbo spin-echo T1WI, spin-echo echo-planar DWI with multiple b-values (50/800/1,500 s/mm^2), and high-resolution isotropic volume with fat suppression T1WI after 0.1 mmol/kg gadodiamide (GE Healthcare, Ireland) injection were employed for dynamic contrast-enhanced (DCE) images. Specific scanning parameters are listed in Electronic Supplementary Material Table S1. Subsequently, ADC maps were generated from DWI using the Philips WorkStation software (United Imaging, Shanghai, China).

Whole-mount histopathology

After prostatectomy, prostate specimens were sectioned from apex to base at 3-mm intervals, followed by paraffin embedding and haematoxylin–eosin staining. All sections were digitised at 200× magnification with a whole-slide scanner (NanoZommer-S60, HAMAMATSU, Japan). All digital sections were reviewed in consensus by two urological pathologists, and each lesion was outlined on multiple sections and assigned a GS including the proportion of different grades. The index lesion was defined as the lesion with the highest GS. When multiple lesions had the same score, the largest was considered as the index lesion.[2] A clinically significant lesion was defined as a lesion with a pathological GS of >6 or volume >0.5 ml,[23,24] which was mostly adopted for RP specimens as recently reviewed by Matoso *et al.*[25]

MRI analysis

All MRI images were reviewed in consensus by two radiologists (with 10 years and 5 years of experience in prostate MRI reading). According to the Prostate Imaging-Reporting and Data System v2 (PI-RADS v2),[6] each lesion was assigned a PI-RADS score according to the T2WI, DWI, ADC, and DCE images, and each lesion suspicious of PCa (PI-RADS≥3) was reported blind to the histopathological results. Further, each lesion outlined on whole-mount sections was matched to the corresponding mpMRI suspicious lesions by comparing the specific location, slide number, and identifiable anatomical landmarks (such as urethra, ejaculatory ducts and benign prostatic hyperplasia). Histologically confirmed tumours corresponding to a previously identified lesion on mpMRI was considered detected. Of clinically significant tumour foci on pathological sections, regions of interest (ROIs) best aligned with the tumour identified on the specimen were drawn on the corresponding matched MRI images by the two radiologists mentioned above in consensus, including both visible lesions and invisible lesions. Representative cases are shown in Fig 2. Briefly, freehand ROIs were drawn on multiple transverse T2 images with software MIStar (Apollo Medical Imaging Technology, Australia) and automatically transferred to both the ADC map and DCE images (prior rigid registration was done to correct patient motion). Pixel-

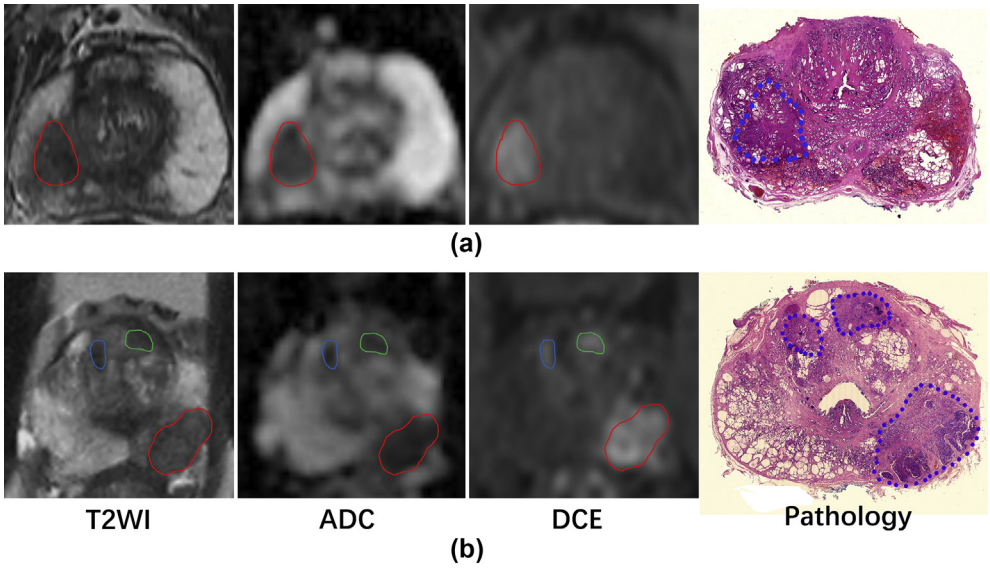

Figure 2 Representative images of radio-pathological matching cases. (a) A 59-year-old man with unifocal PCa (biopsy GS 3+4, PSA level 9.70 ng/ml). Transverse T2WI and ADC map both showed a hypointense area in the right PZ, displaying early enhancement on corresponding DCE image. The lesion was assigned PI-RADS 4. Whole-mount histopathology indicated adenocarcinoma with GS 3+4. (b) A 76-year-old man with multifocal PCa (biopsy GS 4+4, PSA level 51.89 ng/ml). Transverse T2WI and ADC map both showed three hypointense areas in the left PZ, left TZ and right TZ, while all three lesions displayed early enhancement on corresponding DCE image. The three lesions were assigned PI-RADS 5, PI-RADS 3 and PI-RADS 3, respectively. Whole-mount histopathology indicated adenocarcinoma with GS 4+4 (left PZ), 3+4 (left TZ) and 3+4 (right TZ), respectively. Tumour lesions are outlined with contoured solid lines on mpMRI and dotted areas on pathological section.

based values within whole-lesion volume of interest (VOI) on both the T2WI and ADC maps were extracted. The tumour: muscle T2-weighted SI ratio ($T2_{ratio}$) was defined as the ratio of average T2 values between ROIs in the centre of the tumour and internal obturator muscle.[11] The skewness of T2-weighted SI ($T2_{skewness}$) was defined as:

$$\frac{1}{N}\sum_{i=1}^{N}\left(\frac{S_i-\mu}{\sigma}\right)^3$$

where S_i is SI of the i pixel, μ and σ are the mean and standard deviation of all T2 values within the VOI and N is the total number of pixels within the VOI.[13] Skewness is not influenced by the absolute T2-weighted SI.[13] The average ADC value (ADC_{mean}) and 10th percentile ADC value ($ADC_{10\%}$) were calculated from the histogram of pixel-wise ADC values within the VOI as previously described.[14]

Whole-mount image segmentation

Gland components including epithelium (nuclei and cytoplasm), stroma, and glandular lumen were segmented with the Positive Pixel Count algorithm (ImageScope v9.0, Aperio Technologies, San Diego, California, USA) as described previously.[19,26] A segmentation illustration is shown in Fig 3. After importing the images (.ndpi format), a VOI covering the whole tumour region was drawn with Pen Tool at 200× magnification on multiple images. Two sets of initial hue and window values were used for segmentation (setting 1: 0.08 for hue, 0.55 for window; setting 2: 0.7 for hue, 0.35 for window). Slight adjustment to setting values was applied to minimise incorrect segmentation (median adjustment 0.015; maximum adjustment 0.05). The negative pixels in setting 1 corresponded to nuclei, the positive pixels in setting 2 corresponded to epithelial cells, and negative pixels corresponded to stroma. Cytoplasm pixels were derived by subtracting nucleus pixels from epithelial cell pixels, and lumen pixels were derived by subtracting both positive and negative pixels from total pixels within the ROI. Further, nuclear fraction, epithelial fraction luminal fraction and stromal fraction were divided, while the nuclear-to-cytoplasmic ratio (NCR) was calculated by division between nucleus pixels and cytoplasm pixels.

Statistical analysis

Box plots between mpMRI parameters and GS were plotted, and the Spearman correlation coefficients (ρ) were calculated and compared with using the z test. Based on the results of the normality test, two-tailed t-test or Wilcoxon rank sum tests were performed to assess the difference of the average values of mpMRI parameters between GSs. Receiver operating characteristic (ROC) analysis was used for comparison of mpMRI parameters in differentiating GS 6 from GS ≥7, with the corresponding area under the curve (AUC) values and cut-off values. AUC values of different mpMRI parameters were compared using the method by Delong *et al.*[27] The Pearson correlation coefficient (r) was calculated for correlation of mpMRI parameters with cellularity metrics and gland components. Statistical analysis was performed with SPSS 21.0 software (IBM, New York City, New York, USA). All tests were two-sided, with statistical significance set at $p<0.05$.

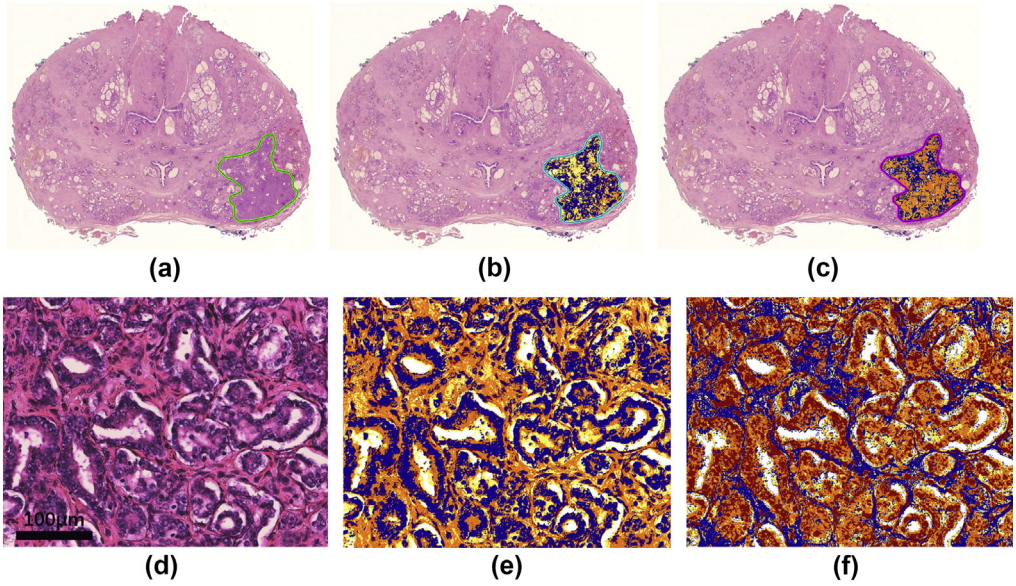

Figure 3 Gland components segmentation with haematoxylin–eosin stained whole-mount prostate sections from a 66-year-old man with PCa (GS 3+4, PSA level 5.97 ng/ml). (a–c) Segmentation illustration of the entire tumour region with whole-mount section (specific segmentation details are not applicable due to low resolution). (d–f) Segmentation illustration of zoomed portion of digitised histological image at 200× magnification (specific segmentation details are available). (b, e) Segmentation of nuclei (blue, negative) with setting 1. (c, f) Segmentation of epithelial cells (orange and red, positive) and stroma (blue, negative) with setting 2. The lumen is white on both segmentation images. Nuclear fraction=0.319, epithelial fraction=0.664, luminal fraction=0.076, stromal fraction=0.260, nuclear-to-cytoplasmic ratio=0.927.

Results

Detection rates of index and clinically significant lesions with mpMRI

Demographic and clinical data of the 225 patients are summarised in Table 1. Solitary lesions were present in 115 patients (51.1%) and the rest were multifocal (48.9%). Lesions distribution was as follows: one focus in 115 of 225 patients (51.1%), two foci in 64 (28.4%), three foci in 32 (14.2%), four foci in 11 (4.9%) and five foci in three (1.4%). Overall, a total of 398 lesions were identified in whole-mount sections, of which 287 (72.1%) were clinically significant lesions. Moreover, a total of 371 suspicious lesions were identified on MRI, with 147/371 (39.6%) of PI-RADS 3, 102/371 (27.5%) of PI-RADS 4, and 122/371 (32.9%) of PI-RADS 5 (Table 1). Of these lesions, 256 were matched on the histopathological sections. Hence, mpMRI demonstrated an overall specificity of 69% (256/371), while the overall sensitivity was 64.3% (256/398), similar in PZ (63.6%) and TZ (66.7%; Table 2). Specifically, 71.5% (123/172) lesions of GS 3+3 were missed, among which 104 (84.6) were non-csPCa. Of the 225 index lesions, 196 (87.1%) were detected, with 87.8% (152/173) in PZ and 84.6% (44/52) in TZ. mpMRI correctly identified 249 of 287 clinically significant lesions (sensitivity 86.8%), including 190 of 217 PZ lesions (sensitivity 87.6%) and 59 of 70 TZ lesions (sensitivity 84.3%).

Table 1
Characteristics of 225 patients with prostate cancer.

Characteristics	Value
Age (years)	70 (65–75)
Preoperative PSA level (ng/ml)	12.23 (7.96–22.24)
Time from MRI to RP (days)	17 (12–27)
Prostate volume (ml)	42 (27.4–50.6)
Index tumour diameter (cm)	2 (1.3–2.7)
PI-RADS score	
3	147 (39.6)
4	102 (27.5)
5	122 (32.9)
Total lesions on MRI	371 (100)
Gleason score of RP	
3+3	36 (16)
3+4	82 (36.4)
4+3	53 (23.6)
≥8	54 (24)
pT stage	
T2	131 (58.2)
T3a	64 (28.4)
T3b	30 (13.4)
pN stage	
N_0	137 (60.9)
N_1	16 (7.1)
N_x	72 (32)
Tumour focality	
Solitary	115 (51.1)
Multifocal	110 (48.9)
Total lesions	398 (100)
PZ	302 (75.9)
TZ	96 (24.1)

Continuous variables are presented as median (interquartile range) and categorical variables are presented as *n* (%).
PSA, prostate specific antigen; RP, radical prostatectomy; PZ, peripheral zone; TZ, transition zone.

Correlation of mpMRI parameters with GS

Clinically significant lesions were selected to further evaluate the relationship between mpMRI parameters and GS. For PZ lesions, $T2_{ratio}$, $T2_{skewness}$, ADC_{mean} and $ADC_{10\%}$ demonstrated significantly negative correlation with GS, while ADC performed better than T2 (maximal ρ: −0.58 versus −0.33; Fig 4, Table 3; z=2.56, p=0.011, data not shown). Similar results were found regarding differentiation between GSs (Electronic Supplementary Material Table S2). Specifically, ADC_{mean} correlated most strongly with GS of lesions in PZ (ρ=−0.58, p<0.001). Of TZ lesions, significant correlation was merely observed between ADC_{mean} and GS (ρ=−0.32, p=0.023), while all parameters failed to differentiate between GSs.

Differentiation of GS 6 from GS ≥7 with mpMRI parameters

Among lesions in PZ, ADC yielded significantly higher AUC values than T2 in differentiating GS 6 from GS ≥7 for PZ lesions (maximal AUC: 0.854 versus 0.731, p=0.020; Fig 5, Electronic Supplementary Material Table S2). Of the ADC parameters, ADC_{mean} showed relatively higher AUC values (0.854 versus 0.848), while no significant differences were found (p-values not shown). With the cut-off value of 667 $\mu m^2/s$, ADC_{mean} differentiated GS 6 from GS ≥7 with a sensitivity of 87% and specificity of 79.3% for PZ lesions (Electronic Supplementary Material Table S3); however, all parameters yielded poor differentiation effectiveness for TZ lesions.

Correlation of mpMRI parameters with cellularity metrics and gland components of PCa

ADC parameters, especially ADC_{mean}, correlated better with NCR and nuclear fraction compared with T2, with significantly moderate relation to NCR and nuclear fraction among PZ lesions (r=−0.403 and −0.514, p<0.001; Fig 6, Table 4). Specifically, correlations of ADC_{mean} with NCR and nuclear fraction were stronger than $ADC_{10\%}$. In addition, of PZ lesions, ADC showed negative correlation with epithelial fraction and positive correlation with luminal fraction as predicted, while in poor correlation with stromal fraction (Table 4). On the contrary, for lesions in TZ, ADC presented moderate correlation with stromal fraction, but no relationship with luminal fraction. Generally, among these cellularity metrics and gland components, epithelial fraction correlated most strongly with ADC (Table 4).

Discussion

In the present study, mpMRI revealed high sensitivities for detection of index and clinically significant PCa lesions. Compared with T2 parameters, ADC parameters, especially ADC_{mean}, correlated better with GS and cellularity metrics (including NCR and nuclear fraction) among PZ lesions. For TZ lesions, ADC and T2 both demonstrated poor performance.

Table 2
Sensitivity of mpMRI for PCa lesions detection stratified by GS and prostate region.

	Sensitivity, % (*n*/*N*)				
	GS 3+3	GS 3+4	GS 4+3	GS ≥8	Total
All lesions					
PZ	23.6 (29/123)	83.8 (67/80)	95.9 (47/49)	98.0 (49/50)	63.6 (192/302)
TZ	40.8 (20/49)	90.0 (27/30)	100 (11/11)	100 (6/6)	66.7 (64/96)
Total	28.5 (49/172)	85.5 (94/110)	96.7 (58/60)	98.2 (55/56)	64.3 (256/398)
Index lesions					
PZ	54.5 (12/22)	85.2 (52/61)	97.6 (41/42)	97.9 (47/48)	87.9 (152/173)
TZ	57.1 (8/14)	90.5 (19/21)	100 (11/11)	100 (6/6)	84.6 (44/52)
Total	55.5 (20/36)	86.6 (71/82)	98.1 (52/53)	98.1 (53/54)	87.1 (196/225)
Clinically significant lesions					
PZ	71.1 (27/38)	83.8 (67/80)	95.9 (47/49)	98.0 (49/50)	87.6 (190/217)
TZ	65.2 (15/23)	90.0 (27/30)	100 (11/11)	100 (6/6)	84.3 (59/70)
Total	68.9 (42/61)	85.5 (94/110)	96.7 (58/60)	98.2 (55/56)	86.8 (249/287)

Data are presented as a percentage (detected lesions/total lesions).
GS, Gleason score; PZ, peripheral zone; TZ, transition zone.

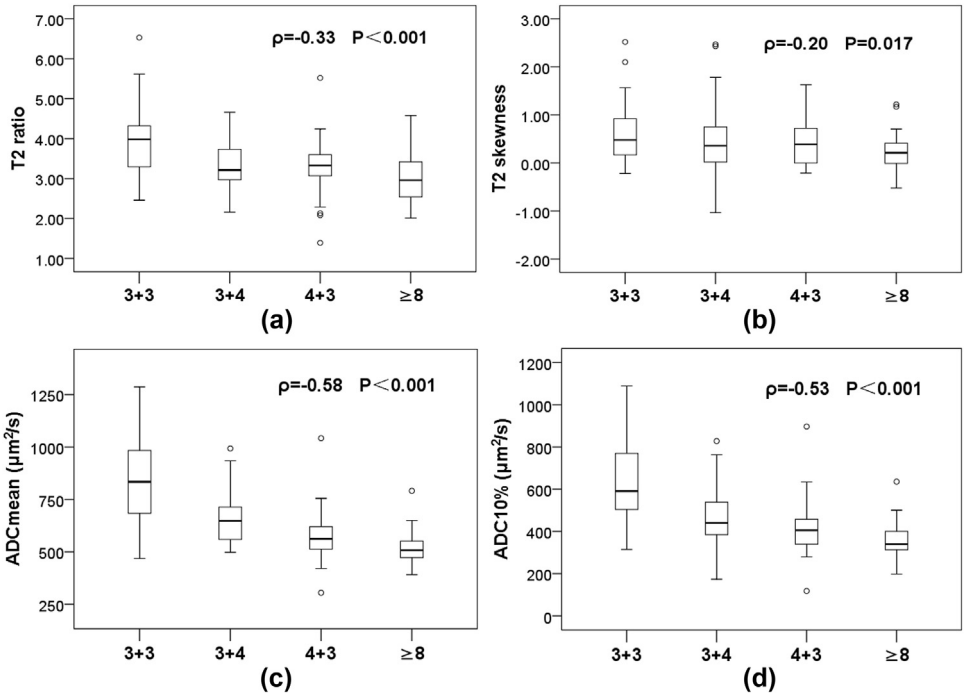

Figure 4 Box plots show correlation of mpMRI parameters with GS for PZ lesions. Line in box is median, height of box represents interquartile range, whiskers are lowest and highest data points still within 1.5 interquartile range, and circles indicate outliers. (a) $T2_{ratio}$ & GS, (b) $T2_{skewness}$ & GS, (c) ADC_{mean} & GS, (d) $ADC_{10\%}$ & GS. ρ: Spearman correlation coefficient.

Table 3
Quantitative analysis and correlation of mpMRI parameters with GS stratified by prostate region.

	GS 3+3	GS 3+4	GS 4+3	GS ≥8	ρ[SD] (*p*-value)
PZ lesions					
$T2_{ratio}$	3.98 (3.29–4.44)	3.21 (2.96–3.73)	3.33 (2.97–3.61)	2.96 (2.52–3.46)	−0.33 [0.081] (<0.001)
$T2_{skewness}$	0.48 (0.14–1.01)	0.36 (0.02–0.82)	0.38 (0.0–0.75)	0.21 (−0.02–0.4)	−0.20 [0.082] (0.017)
ADC_{mean}	834 (682–988)	648 (559–717)	564 (513–626)	508 (468–556)	−0.58 [0.060] (<0.001)
$ADC_{10\%}$	591 (504–786)	441 (380–545)	409 (338–459)	340 (308–401)	−0.53 [0.066] (<0.001)
TZ lesions					
$T2_{ratio}$	3.24 (2.52–3.63)	3.29 (2.59–3.66)	2.90 (2.72–3.35)	3.16 (2.48–3.26)	−0.08 [0.132] (0.554)
$T2_{skewness}$	0.30 (0.16–0.62)	0.47 (0.28–1.25)	0.05 (−0.5–0.1)	0.07 (0.03–1.10)	−0.18 [0.140] (0.208)
ADC_{mean}	767 (620–892)	696 (588–782)	589 (490–728)	581 (562–727)	−0.32 [0.133] (0.023)
$ADC_{10\%}$	591 (454–723)	544 (428–657)	455 (344–641)	473 (381–610)	−0.24 [0.143] (0.087)

Data are presented as median (interquartile range). Units: ADC_{mean}/$ADC_{10\%}$: $\mu m^2/s$.
GS, Gleason score; PZ, peripheral zone; TZ, transition zone; ADC, apparent diffusion coefficient; ρ: Spearman correlation coefficient; SD, standard deviation.

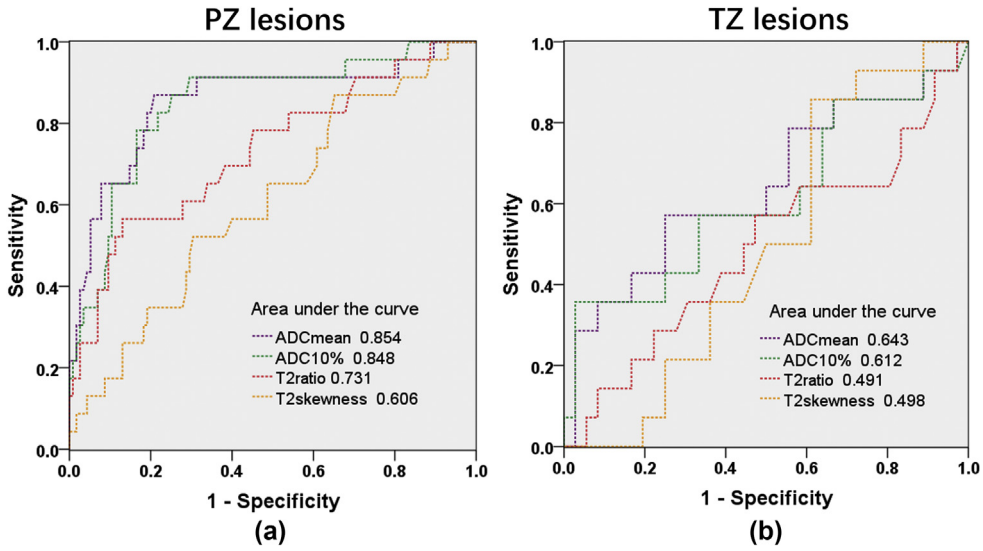

Figure 5 ROC curves for comparison of different mpMRI parameters in differentiating GS 6 from GS ≥7 among PZ lesions (a) and TZ lesions (b).

Characterised as heterogeneous and frequently multifocal disease, PCa with different cell clones indicated different prognosis, while index lesions and clinically significant lesions tended to dominate the oncology behaviours.[3–5] The present study verified that mpMRI was able to detect the majority of index and clinically significant PCa, with analogical detection rates between PZ and TZ. The present results are similar to the study of Russo *et al.*,[28] which presented sensitivities of 90.4%, 85.5%, 63.6% for index, clinically significant, and all lesions, respectively; however, the definition of index lesion by Russo *et al.* (lesion with the largest volume) was different from the present study (lesion with the highest GS), which needs to be noted. With the same definition of index lesion, lower sensitivities for index lesion (80%) and all lesions (47%) were reported by Le *et al.*[2] The relatively larger index tumour size of the present series might contribute to higher detection rates according to the result by Le *et al.*[2]

Further, non-invasive methods of predicting PCa aggressiveness are necessary for diagnosis and treatment. A previous study revealed that $T2_{ratio}$ significantly correlated with Gleason grade[3,4 and 5] for PZ tumours,[11] while weak correlation with GS was observed in the present series. The heterogeneous composition of GS rather than single Gleason grade might be the interpretation. $T2_{skewness}$ quantifies the relative number of dark pixels versus bright pixels within a ROI, with potential for differentiation of PCa foci from normal prostate tissue.[13] A study by Peng *et al.* showed that $T2_{skewness}$ could differentiate PCa from normal PZ tissue with an AUC of 0.86.[12] In addition, as a common feature of texture analysis, skewness demonstrated excellent performance in Crohn's diseases,[29] bone carcinoma[30] and rectal cancer[31] with MRI images; however, there was poor correlation between $T2_{skewness}$ and GS of lesions in both PZ and TZ in the present cohort, which might be explained by relatively homogeneous T2 signal intensities within tumour. Better than T2, ADC presented significantly negative correlation with GS and significantly higher AUC values in differentiating GS 6 from GS ≥7 for PZ lesions, consistent with previous studies.[12–14] This is in line with how the PI-RADS evaluation is structured, where diffusion is the primary consideration for PZ lesions, but not for TZ lesions.[6] Specifically, several studies compared the effectiveness between ADC_{mean} and $ADC_{10\%}$ for evaluation of PCa aggressiveness. Donati *et al.*[14] reported that $ADC_{10\%}$ performed better than ADC_{mean} with whole-volume analysis, while Peng *et al.* presented different results in two separate datasets.[13] In the present cohort, ADC_{mean} correlated most strongly with GS and yielded relatively higher AUC values than $ADC_{10\%}$ with whole-volume analysis. Generally, ADC_{mean} was expected to help characterise restricted water diffusion in tumours, while $ADC_{10\%}$ was expected to help identify sparse tumours intermixed with normal tissue.[13,32] Therefore, the diagnostic efficiency varies among different types of tumour composition. In the authors' opinion, $ADC_{10\%}$ mostly represents the highest Gleason grade within a ROI, which might narrow the gap between Gleason scores (such as 3+4 versus 4+4). Further research is necessary for the comparison. Notably, different from Donati *et al.*,[14] poor correlation was observed between mpMRI parameters and GS for lesions originating in the TZ. Thus, special attention should be paid to TZ lesions when using MRI for risk stratification.

Historically, alterations in number and size of nuclei have been recognised as an early indication of cancer,[33] and changes in the number and size of nuclei distinguish benign from metastatic PCa, while the latter are characterised by the presence of enlarged nuclei that are particularly pronounced in high-grade tumours.[18,34] Generally, high-grade tumours are associated with poorly differentiated and often packed epithelial cells compared with low-grade tumours that have at least some individual glandular structures and intercellular space,[35] which induces reduced ADC values. Hence, the relationship between ADC and cellularity metrics was investigated in the present study, yielding moderate correlation with NCR and nuclear fraction.

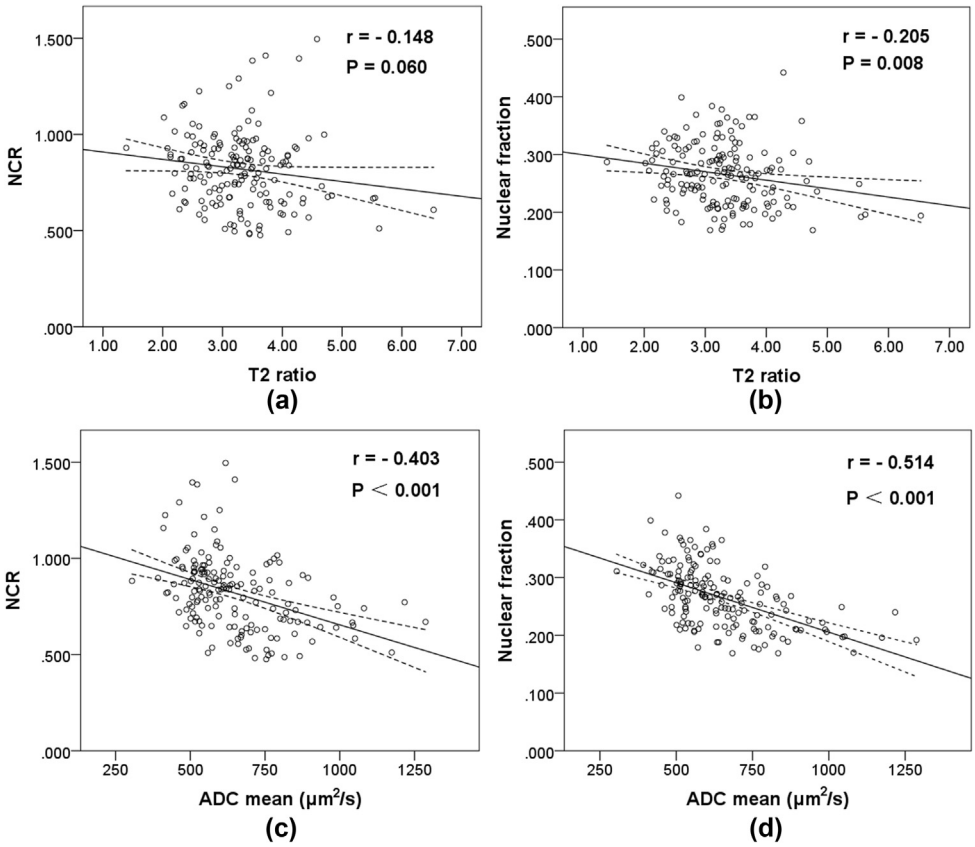

Figure 6 Graphs show correlation of cellularity metrics (NCR and nuclear fraction) with $T2_{ratio}$ and ADC_{mean} among PZ lesions. (a) NCR & $T2_{ratio}$, (b) nuclear fraction & $T2_{ratio}$, (c) NCR & ADC_{mean}, (d) Nuclear fraction & ADC_{mean}. Dotted lines indicate 95% confidence intervals. NCR, nuclear-to-cytoplasmic ratio; r, Pearson correlation coefficient.

Table 4
Pearson correlation of mpMRI parameters with cellularity metrics and gland components stratified by prostate region.

	NCR	Nuclear fraction	Epithelial fraction	Luminal fraction	Stromal fraction
PZ lesions					
$T2_{ratio}$	−0.148 [0.060]	−0.205 [0.008]	−0.292 [0.001]	0.321 [0.000]	−0.003 [0.974]
$T2_{skewness}$	−0.238 [0.002]	−0.219 [0.005]	−0.173 [0.059]	0.137 [0.132]	0.088 [0.334]
ADC_{mean}	−0.403 [0.000]	−0.514 [0.000]	−0.524 [0.000]	0.477 [0.000]	0.209 [0.020]
$ADC_{10\%}$	−0.341 [0.000]	−0.427 [0.000]	−0.476 [0.000]	0.462 [0.000]	0.089 [0.332]
TZ lesions					
$T2_{ratio}$	−0.101 [0.536]	−0.194 [0.231]	−0.144 [0.382]	0.327 [0.039]	−0.164 [0.312]
$T2_{skewness}$	−0.330 [0.040]	−0.217 [0.185]	−0.012 [0.941]	0.096 [0.559]	0.096 [0.559]
ADC_{mean}	−0.347 [0.029]	−0.389 [0.012]	−0.631 [0.000]	0.195 [0.228]	0.481 [0.002]
$ADC_{10\%}$	−0.343 [0.031]	−0.364 [0.018]	−0.566 [0.000]	0.121 [0.458]	0.477 [0.002]

Data are presented as r [*p*-value].
NCR, nuclear-to-cytoplasmic ratio; ADC, apparent diffusion coefficient; PZ, peripheral zone; TZ, transition zone.

Negative correlation between ADC and nuclear fraction were verified in several articles, with correlation coefficient ranging from −0.29 to −0.57.[20,22,36] To the authors' knowledge, the relationship between ADC and NCR was reported by Hectors *et al.* in 24 PCa patients but no correlation was found,[26] while there was moderate correlation in the present larger series. Simultaneously, epithelial fraction correlated most strongly with ADC parameters, consistent with previous study.[20] Interestingly, of the luminal fraction, moderate correlation with ADC was observed for the PZ lesions but poor correlation among TZ lesions. For the stromal fraction, the results were just the opposite. The hypothesis of the present study was that different proportions of glandular tissue in the PZ (70–80%) and TZ (5%)[6] determined the luminal and stromal contribution weightiness to ADC values.

Using whole-mount histopathology as the reference standard is a major strength of the present study, to allow an exact match between MRI and RP specimens. In addition, 225 PCa patients, who underwent same MRI manipulation protocol, were enrolled to compare the diagnostic performance of different parameters for GS and cellularity metrics

(including novel NCR) of lesions in the PZ and TZ separately, whereas most of the previous studies took them as a whole; however, the study has some potential limitations. First, it is a retrospective study from a single institution, thus the present findings need to be validated in prospective and multicentric studies. Second, selection bias exists referring to enrolling RP patients with whole-mount histopathology. Patients with biopsy pathology of clinically insignificant PCa would choose active surveillance, thus data of such patients were not available, and caution should be taken when applying the results for such patients. Nonetheless, the final RP specimen is the most accurate arbiter for pathological evaluation on a per-lesion analysis. Third, although nearly 300 lesions were included for quantitative analysis, due to the relative lack of lesions originating from the TZ, the corresponding results need to be verified in a larger series.

In summary, index and clinically significant PCa could be effectively detected using mpMRI with similar or higher sensitivities compared with previous studies. For PZ lesions, quantitative analysis revealed that ADC parameters correlated better with GS and cellularity metrics than T2 parameters, while ADC_{mean} performed better than $ADC_{10\%}$ in the present study group. Notably, all parameters demonstrated poor performance within lesions in TZ. These results could be used for risk stratification at the time of diagnosis and index lesion selection for biopsy or focal therapy within patients suspicious of PCa. Patients of radiologically low-risk PCa could be considered for active surveillance while avoiding biopsy or focal therapy.

Conflict of interest

The authors declare no conflict of interest.

Acknowledgements

This research was supported by the National Natural Science Foundation of China (grant nos. 81772710, 81572519, 81802535 and 81602221) and the Project of Invigorating Health Care through Science, Technology and Education, Jiangsu Provincial Key Medical Discipline (Laboratory; ZDXKB2016014), the National Natural Science Foundation of Jiangsu Province (BK20160117), China Postdoctoral Fund (223427) and Nanjing Medical Science and technique Development Foundation (YKK 18064).

Appendix A. Supplementary data

Supplementary data to this article can be found online at https://doi.org/10.1016/j.crad.2019.06.012.

References

1. Siegel RL, Miller KD, Jemal A. Cancer statistics, 2017. *CA Cancer J Clin* 2017;**67**(1):7–30.
2. Le JD, Tan N, Shkolyar E, *et al*. Multifocality and prostate cancer detection by multiparametric magnetic resonance imaging: correlation with whole-mount histopathology. *Eur Urol* 2015;**67**(3):569–76.
3. Ahmed HU, Hu Y, Carter T, *et al*. Characterizing clinically significant prostate cancer using template prostate mapping biopsy. *J Urol* 2011;**186**(2):458–64.
4. Ahmed HU. The index lesion and the origin of prostate cancer. *N Engl J Med* 2009;**361**(17):1704–6.
5. Liu W, Laitinen S, Khan S, *et al*. Copy number analysis indicates monoclonal origin of lethal metastatic prostate cancer. *Nat Med* 2009;**15**(5):559–65.
6. Weinreb JC, Barentsz JO, Choyke PL, *et al*. PI-RADS prostate imaging - reporting and data system: 2015, version 2. *Eur Urol* 2016;**69**(1):16–40.
7. Ahmed HU, El-Shater Bosaily A, Brown LC, *et al*. Diagnostic accuracy of multi-parametric MRI and TRUS biopsy in prostate cancer (PROMIS): a paired validating confirmatory study. *Lancet* 2017;**389**(10071):815–22.
8. Kasivisvanathan V, Rannikko AS, Borghi M, *et al*. MRI-targeted or standard biopsy for prostate-cancer diagnosis. *N Engl J Med* 2018;**378**(19):1767–77.
9. Radtke JP, Hadaschik BA, Wolf MB, *et al*. The impact of magnetic resonance imaging on prediction of extraprostatic extension and prostatectomy outcome in patients with low-, intermediate- and high-risk prostate cancer: try to find a standard. *J Endourol* 2015;**29**(12):1396–405.
10. Mottet N, Bellmunt J, Bolla M, *et al*. EAU-ESTRO-SIOG guidelines on prostate cancer. Part 1: screening, diagnosis, and local treatment with curative intent. *Eur Urol* 2017;**71**(4):618–29.
11. Wang L, Mazaheri Y, Zhang J, *et al*. Assessment of biologic aggressiveness of prostate cancer: correlation of MR signal intensity with Gleason grade after radical prostatectomy. *Radiology* 2008;**246**(1):168–76.
12. Peng Y, Jiang Y, Yang C, *et al*. Quantitative analysis of multiparametric prostate MR images: differentiation between prostate cancer and normal tissue and correlation with Gleason score—a computer-aided diagnosis development study. *Radiology* 2013;**267**(3):787–96.
13. Peng Y, Jiang Y, Antic T, *et al*. Validation of quantitative analysis of multiparametric prostate MR images for prostate cancer detection and aggressiveness assessment: a cross-imager study. *Radiology* 2014;**271**(2):461–71.
14. Donati OF, Mazaheri Y, Afaq A, *et al*. Prostate cancer aggressiveness: assessment with whole-lesion histogram analysis of the apparent diffusion coefficient. *Radiology* 2014;**271**(1):143–52.
15. Pierre T, Cornud F. Diffusion-weighted imaging of the prostate: should we use quantitative metrics to better characterize focal lesions originating in the peripheral zone? *Eur Radiol* 2018;**28**(5):2236–45.
16. Hambrock T, Somford DM, Huisman HJ, *et al*. Relationship between apparent diffusion coefficients at 3.0-T MR imaging and Gleason grade in peripheral zone prostate cancer. *Radiology* 2011;**259**(2):453–61.
17. Wang XZ, Wang B, Gao ZQ, *et al*. Diffusion-weighted imaging of prostate cancer: correlation between apparent diffusion coefficient values and tumour proliferation. *J Magn Reson Imaging* 2009;**29**(6):1360–6.
18. Humphrey P. *Prostate pathology*. Chicago: American Society of Clinical Pathologists Press; 2003.
19. Langer DL, van der Kwast TH, Evans AJ, *et al*. Prostate tissue composition and MR measurements: investigating the relationships between ADC, T2, K(trans), v(e), and corresponding histologic features. *Radiology* 2010;**255**(2):485–94.
20. Chatterjee A, Watson G, Myint E, *et al*. Changes in epithelium, stroma, and lumen space correlate more strongly with Gleason pattern and are stronger predictors of prostate ADC changes than cellularity metrics. *Radiology* 2015;**277**(3):751–62.
21. Venkataraman G, Rycyna K, Rabanser A, *et al*. Morphometric signature differences in nuclei of Gleason pattern 4 areas in Gleason 7 prostate cancer with differing primary grades on needle biopsy. *J Urol* 2009;**181**(1):88–93. discussion 93-84.
22. Zelhof B, Pickles M, Liney G, *et al*. Correlation of diffusion-weighted magnetic resonance data with cellularity in prostate cancer. *BJU Int* 2009;**103**(7):883–8.
23. Stamey TA, Freiha FS, McNeal JE, *et al*. Localized prostate cancer. Relationship of tumour volume to clinical significance for treatment of prostate cancer. *Cancer* 1993;**71**(3 Suppl):933–8.
24. Priester A, Natarajan S, Khoshnoodi P, *et al*. Magnetic resonance imaging underestimation of prostate cancer geometry: use of patient specific molds to correlate images with whole mount pathology. *J Urol* 2017;**197**(2):320–6.

25. Matoso A, Epstein JI. Defining clinically significant prostate cancer on the basis of pathological findings 2019;**74**(1):135–45.
26. Hectors SJ, Semaan S. Advanced Diffusion-weighted imaging modeling for prostate cancer characterization: correlation with quantitative histopathologic tumour tissue composition—a hypothesis-generating study 2018;**286**(3):918–28.
27. DeLong ER, DeLong DM, Clarke-Pearson DL. Comparing the areas under two or more correlated receiver operating characteristic curves: a nonparametric approach. *Biometrics* 1988;**44**(3):837–45.
28. Russo F, Regge D, Armando E, *et al*. Detection of prostate cancer index lesions with multiparametric magnetic resonance imaging (mp-MRI) using whole-mount histological sections as the reference standard. *BJU Int* 2016;**118**(1):84–94.
29. Makanyanga J, Ganeshan B, Rodriguez-Justo M, *et al*. MRI texture analysis (MRTA) of T2-weighted images in Crohn's disease may provide information on histological and MRI disease activity in patients undergoing ileal resection. *Eur Radiol* 2017;**27**(2):589–97.
30. Lisson CS, Lisson CG, Flosdorf K, *et al*. Diagnostic value of MRI-based 3D texture analysis for tissue characterisation and discrimination of low-grade chondrosarcoma from enchondroma: a pilot study. *Eur Radiol* 2018;**28**(2):468–77.
31. Oh JE, Kim MJ, Lee J, *et al*. Magnetic resonance-based texture analysis differentiating KRAS mutation status in rectal cancer. *Cancer Res Treat* 2019; May 7, https://doi.org/10.4143/crt.2019.050 [Epub ahead of print].
32. Langer DL, van der Kwast TH, Evans AJ, *et al*. Intermixed normal tissue within prostate cancer: effect on MR imaging measurements of apparent diffusion coefficient and T2–sparse versus dense cancers. *Radiology* 2008;**249**(3):900–8.
33. Zaidi SK, Young DW, Javed A, *et al*. Nuclear microenvironments in biological control and cancer. *Nat Rev Cancer* 2007;**7**(6):454–63.
34. Fischer AH, Bardarov Jr S, Jiang Z. Molecular aspects of diagnostic nucleolar and nuclear envelope changes in prostate cancer. *J Cell Biochem* 2004;**91**(1):170–84.
35. Epstein JING. *Biopsy interpretation of the prostate*. 4th edn. Philadelphia, PA: Lippincott Williams & Wilkins; 2007. p. 175–202.
36. Kobus T, van der Laak JA, Maas MC, *et al*. Contribution of histopathologic tissue composition to quantitative MR spectroscopy and diffusion-weighted imaging of the prostate. *Radiology* 2016;**278**(3):801–11.